Applied Energy 195 (2017) 738–753

Contents lists available at ScienceDirect

Applied Energy

journal homepage: www.elsevier.com/locate/apenergy

Prediction of electric vehicle charging-power demand in realistic urban traffic networks

Mariz B. Arias [a,b], Myungchin Kim [c], Sungwoo Bae [a,*]

[a] Department of Electrical Engineering, Hanyang University, Seoul 04763, South Korea
[b] Department of Electrical Engineering, University of Santo Tomas, España, Manila 1015, Philippines
[c] School of Electrical Engineering, Chungbuk National University, Cheongju 28644, South Korea

HIGHLIGHTS

- A time-spatial EV charging-power demand forecast model in urban areas is proposed.
- Charging-power demand at different fast-charging rates is predicted by the model.
- Different EV charging patterns at various charging stations are analyzed.
- A Markov-chain traffic modeling is used with an actual urban road network.
- Real-time CCTV data are used for an urban traffic pattern analysis.

ARTICLE INFO

Article history:
Received 17 October 2016
Received in revised form 24 January 2017
Accepted 8 February 2017
Available online 31 March 2017

Keywords:
Electric vehicle charging-power demand
Markov-chain traffic model
Charging patterns
Real-time closed-circuit television data
Urban area

ABSTRACT

This paper presents a time-spatial electric vehicle (EV) charging-power demand forecast model at fast-charging stations located in urban areas. Most previous studies have considered private charging locations and a fixed charging-start time to predict the EV charging-power demand. Few studies have considered predicting the EV charging-power demand in urban areas with time-spatial model analyses. The approaches used in previous studies also may not be applicable to predicting the EV charging-power demand in urban areas because of the complicated urban road network. To possibly forecast the actual EV charging-power demand in an urban area, real-time closed-circuit television (CCTV) data from an actual urban road network are considered. In this study, a road network inside the metropolitan area of Seoul, South Korea was used to formulate the EV charging-power demand model using two steps. First, the arrival rate of EVs at the charging stations located near road segments of the urban road network is determined by a Markov-chain traffic model and a teleportation approach. Then, the EV charging-power demand at the public fast-charging stations is determined using the information from the first step. Numerical examples for the EV charging-power demand during three time ranges (i.e., morning, afternoon, and evening) are presented to predict the charging-power demand profiles at the public fast-charging stations in urban areas. The proposed time-spatial model can also contribute to investment and operation plans for adaptive EV charging infrastructures with renewable resources and energy storage depending on the EV charging-power demand in urban areas.

© 2017 Elsevier Ltd. All rights reserved.

1. Introduction

Electric vehicles (EVs) have increased in the market as they play a major role in achieving sustainable transportation that addresses future energy requirements. EVs are essential for increasing energy security and reducing the emissions of greenhouse gases and other pollutants [1]. A conversion from internal–combustion-engine (ICE) vehicles to EVs can reduce the dependence on fossil fuels and increase energy security because EVs use off-board electricity sources generated by nuclear fission energy, natural gas, and renewable energy sources [2]. In addition, according to the Electric Vehicle Charging Information System [3], 2.3 tons of carbon dioxide is reduced annually by replacing ICE vehicles with EVs.

According to the electric-power industry, the number of annual EV sales is expected to quadruple by 2023 [4]. However, the high EV penetration may substantially increase the electricity usage and peak power demand in high adoption areas. Therefore, an

* Corresponding author.
E-mail address: swbae@hanyang.ac.kr (S. Bae).

http://dx.doi.org/10.1016/j.apenergy.2017.02.021
0306-2619/© 2017 Elsevier Ltd. All rights reserved.

Nomenclature

CCTV	closed-circuit television
EV	electric vehicle
SOC	battery state-of-charge value
U	teleportation transition matrix
d	probability vector whose element represents the probability that the corresponding road segment is the destination of a route
o	probability vector whose element represents the probability that the corresponding road segment is the origin of a route
w	left-hand Perron eigenvector
N_{ij}	number of vehicles that move from node i to node j
N_{ik}	number of vehicles that pass through node i
$\mathbf{P_a}$	transition matrix in the afternoon time range
$\mathbf{P_e}$	transition matrix in the evening time range
$\mathbf{P_m}$	transition matrix in the morning time range
P_d	charging power of each charger at the charging station on the i^{th} road segment
P_i	total electric vehicle charging-power demand at node i
f_c	probability density function of the charged state-of-charge value
f_{soc}	probability density function of the remaining available state-of-charge value
l_i	length of the road segment at node i
p_{ij}	probability of a transition from state i to state j
t_i	average travel time for the road segment at node i
tp_{ij}	turning probability of going from road segment at node i to road segment at node j
v_i	average vehicle speed on the road segment at node i
α_i	arrival rate at the i^{th} road segment
ρ_i	vehicular density on the i^{th} road segment
μ_c	average charged state-of-charge value
μ_{soc}	average remaining available state-of-charge value
σ_c	standard deviation of the charged state-of-charge value
σ_{soc}	standard deviation of the remaining available state-of-charge value

accurate EV charging-power demand forecast system has been studied and developed to evaluate the impact of charging EV batteries on the power systems.

Several studies [5–17] have assessed this EV charging impact on power distribution systems using both deterministic and stochastic methods. These studies [9–16] have shown that uncontrolled EV charging can have a negative effect by introducing high power demand on the power system. Temiz and Guven [16] assessed the impacts of EV on power distribution systems based on probabilistic models. To accomplish this evaluation, they identified EV-charging characteristics based on different probability distribution functions including Gaussian distribution functions for grid plug-in times for EV charging and Weibull distribution functions for daily vehicle travel times [16]. Other studies [5,14,17,18] also considered real data in determining the EV charging-power demand. In two studies [17,18], real traffic and charging data influenced by weather data were considered in determining the EV charging-power demand. In addition, the integration of sustainable mobility, stationary energy storage systems, and renewable energy sources were also studied in previous studies [19–23]. Studies [21–23] presented the integration of renewable energy sources in the EV charging infrastructures.

However, most previous works have investigated settings that consider private charging locations and a fixed charging-start time. While such settings are valid for predicting the charging-power demand of EVs that are parked at a private charging spot during a specified time period (e.g., vehicles that are charged at homes or at workplaces), such settings cannot be used to characterize the charging-power demand of EVs that are charged at public fast-charging stations. Therefore, models that characterize the time-spatial charging-power demand of EVs at public charging stations should be developed so that the EV charging-power demand can be predicted more accurately and reliably.

However, only a few studies [14,24–27] have presented a time-spatial EV charging–power demand prediction model. Bae and Kwasinski [24] presented a time-spatial EV charging-power demand anticipation study that considered a Poisson-distributed vehicle arrival rate at fast-charging stations near highway exits, and estimated the EV charging-power demand based on an M/M/s queueing theory. Shrestha and Hansen [25] presented a state-transition algorithm that was used to develop a stochastic model of EV movement in an integrated traffic and power network.

Considering the increased use of EVs in metropolitan areas, researchers [14,26,27] also studied EV charging-power demand models for urban settings. Mu et al. [14] developed a time-spatial model that integrated a transportation analysis into a power-system analysis. Zhou and Lin [26] presented a time-based EV charging-power demand forecast model with multiple charging stations in an urban area. They anticipated the EV arrival rate at a charging station with a cell-transmission traffic model and used an M/M/s queue for the EV charging service. Viswanathan et al. [27] evaluated the time-spatial aspect of the charging-station placement using modeling and simulation based on real-world traffic data.

As the EV penetration rate increases, the need for developing time-spatial EV charging-power demand models that consider the uniqueness of urban areas is expected to grow. The rather high complexity of road networks and traffic flow in realistic urban areas is expected to introduce challenges for applying the models and approaches of previous studies. In addition, EV charging-power demand models for urban areas should consider that the road system is populated with vehicles, and EV users can charge their EVs at a fast-charging station whenever they have not charged their batteries at home or work. Although using EVs in urban neighborhoods is expected to be non-negligible, only a few studies [14,26,27] on determining the EV charging-power demand in urban areas have been reported.

This paper presents a time-spatial EV charging-power demand prediction model for fast-charging stations in realistic urban traffic networks. An urban road network located at the center of Seoul, South Korea is used to formulate the EV charging-power demand model using two steps. The first step is to determine the vehicle arrival rate at EV charging stations based on a Markov-chain traffic model. A Markov chain [28,29] is used to describe the urban road network as presented in [30] such that the traffic data (i.e., arrival rate) of each road segment are determined. Then, the EV charging-power demand at public fast-charging stations on the urban road network is estimated using traffic information and EV battery-charging information. Based on the developed approach, the charging-power demand of EVs that arrive at the fast-charging stations with a relatively low state-of-charge (SOC) level (i.e., between or equal to 0.2 and 0.3) is predicted for three time ranges including morning, afternoon, and evening (i.e., 7:00–9:00, 12:00–14:00, and 17:00–19:00). The owners of EVs that need charging are expected

to charge their EVs at public fast-charging stations to reach their destinations.

Compared with past studies on EV charging-power demand modeling in urban areas, the contributions of this paper include the following.

(i) This study introduced an urban road-network model based on a Markov-chain traffic model to describe the EV arrival rate at specific fast-charging stations. Although a previous study [29] used a Markov decision process to describe an optimal EV charging strategy, its focus was on developing an optimal charging strategy for an EV, whereas our study investigated an approach for predicting the EV charging-power demand that involved the traffic flow of multiple EVs. Furthermore, our study considered an actual urban road network to determine the traffic patterns in urban areas. Real-time data collected from CCTVs located at road segments of the chosen urban road network were used to predict the EV charging-power demand at public fast-charging stations. The average travel time, turning probability, origin probability, destination probability, and average speed at the road segments were used as parameters to determine the EV arrival rate at the charging stations. Different from previous studies [14,24–26], the real-time traffic data were collected from an actual urban road network rather than using mathematical models to determine the EV charging-power demand. Hence, the results of this paper more realistically characterize the EV charging-power demand pattern of metropolitan areas.

(ii) In addition, this study introduced an approach that can be generalized to most urban areas. The discussion is not limited by considering only private charging locations and a fixed charging period, but is expanded by including public fast-charging facilities and observing real-time data of various time periods. As a case study, this paper considered an actual urban road network with two fast-charging stations that were in service. To study how different time periods over one day could affect the EV charging-power demand, three different time periods (i.e., morning, afternoon, and evening) were considered. Compared with most previous research works [5–7] which considered private charging locations and fixed charging-start times, this study investigated how changes in both charging locations and charging time periods would affect the EV charging-power demand in urban areas.

(iii) This study also performed a comprehensive analysis on the effect of different EV operation patterns (i.e., charging profiles) on the power-load demand. While most previous studies only investigated fixed charging patterns [12,13,18], patterns that assumed that all EVs were fully charged [5,7,8,10,11], or random charging [14,25], this study investigated various combinations of these charging patterns. Since the cost of charging EVs is non-negligible, these charging patterns will be factors that could influence the EV charging-power demand.

The remainder of the paper is structured as follows: the relationships of a Markov chain to a theoretic graph, a road network, and a teleportation approach are presented in Section 2. Details on the considered urban road network, the model formulation approach based on a Markov-chain urban traffic model, the charging-power demand calculation approach, and EV charging characteristics are presented in Section 3. Numerical examples are presented in Section 4 to illustrate the effectiveness of our time-spatial model of the EV charging-power demand. Finally, Section 5 concludes this paper with a summary of our findings.

2. Markov chain

Many studies [31–34] have discussed the importance of pattern modeling. In this study, a Markov chain is used for spatial forecasting modeling. Several studies [35–44] have discussed the usefulness of a Markov chain for developing spatial forecasting models. Different applications of spatial forecasting modeling based on a Markov chain have been shown in previous studies [35–44]. For instance, Bojesen et al. [43] presented a spatial representation of forecasting biogas production, while Saadi et al. [44] developed an integrated framework in forecasting travel behavior based on a Markov chain. In this paper, Markov chain theory [28–30,45] is used for traffic modeling to forecast the EV charging demand. This section explains the role of a Markov chain in traffic modeling and the relationship of a Markov chain to a graph [46] and a road network.

In this paper, the urban road network will be described using a transition matrix based on a Markov chain [28–30,45]. The Markov chain, which is commonly used for discrete time stochastic processes, can be characterized as [28–30,45]:

$$p(x_{k+1} = S_{k+1} | x_k = S_k, x_{k-1} = S_{k-1}, \ldots, x_0 = S_0) = p(x_{k+1} = S_{k+1} | x_k = S_k), \quad (1)$$

which means that the probability that x, a random variable, belongs to state S_{k+1} at time step $k+1$ is determined, not by values from previous time steps, but the state of x at time step k. This paper uses a finite-state and discrete-time homogeneous Markov chain. The considered Markov chain is defined by an $n \times n$ transition-probability matrix $\mathbf{P}$, whose elements p_{ij} represent the probability of a transition from state S_i to state S_j, and n stands for the number of states. The elements are non-negative and the sum of each row is equal to 1, which satisfies a stochastic matrix. This Markov chain can be represented by a state-transition diagram. The state-transition diagram shown in Fig. 1 is a finite directed graph in which state i is depicted by a vertex and a conversion from state i to state j is denoted by an edge with transition probability p_{ij}. In this study, the urban road network is presented as a graph modeled by the state-transition matrix using a Markov chain and a graph presented in the following sections.

2.1. Markov chain and graph theory

A graph, as shown in Fig. 1, is composed of a non-empty set of nodes and edges [46]. The corresponding graph is described by a set of nodes linked through edges. The graph can also visually represent the system behavior of a given transition matrix $\mathbf{P}$. Given a finite set of n nodes where, for each pair of nodes $i, j = 1, \ldots, n$, an edge from node i to node j denotes a direct transition from state i to state j in the Markov chain, if and only if $p_{ij} \neq 0$. For example, the graph shown in Fig. 1 can be represented by transition matrix $\mathbf{P}$ as:

$$\mathbf{P} = \begin{bmatrix} p_{11} & p_{12} & 0 & 0 \\ p_{21} & 0 & p_{23} & 0 \\ p_{31} & 0 & 0 & p_{3n} \\ 0 & 0 & p_{n3} & p_{nn} \end{bmatrix} \quad (2)$$

where p_{ij} is the probability that the system will transit from state i to state j. The zero elements show no connection between the nodes in the graph.

A graph has a strong connectivity if, for each pair of nodes, it is possible to reach any other nodes of the graph using the directed edges and, if and only if the graph is irreducible. The Perron–Frobenius theorem, which describes some properties of irreducible transition matrices [30], is applied in this study. In particular, an essential property to be used in our study is that there exists a

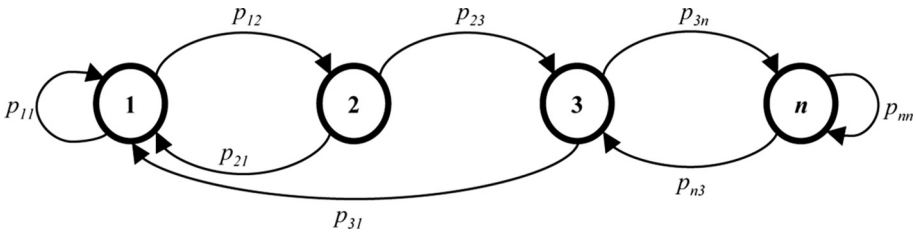

Fig. 1. Markov-chain state-transition diagram.

unique vector $\boldsymbol{w}$, also known as a left-hand Perron eigenvector, which satisfies $\boldsymbol{w}^T\mathbf{P} = \boldsymbol{w}^T$, $\|\boldsymbol{w}\|_1 = 1$, and $\boldsymbol{w} > 0$. Furthermore, the i^{th} component value of the left-hand Perron eigenvector (i.e., w_i) is the probability that the considered system will be in state S_i after a fair amount of time (i.e., steady state). In fact, row vector $\boldsymbol{w}^T$ is also known as the stationary distribution vector [30]. Such a row vector will be used to describe the vehicular density of a road segment and is further explained in Section 3. Additional discussions on interesting properties of irreducible transition matrices, e.g., the spectral radius of the transition matrix $\mathbf{P}$, Perron root, and algebraic multiplicity, can be found in [30].

2.2. Markov chain and road network

In order to represent road networks using a Markov chain approach, the urban road network is interpreted as a directed graph in this study. In urban studies, the network approach has been widely used to perform economic and transportation analyses [47]. The network approach provides a simple and intuitive method to describe complex networks in which nodes relate to junctions and edges represent the connecting roads between the junctions. The resulting graph is called the primal graph representation [47]. Fig. 2(a) shows the primal representation of the urban road network considered in this paper. It is located at the center of Seoul, South Korea. The investigated urban road network in which two EV charging stations are located as depicted in Fig. 2(a) is approximately 1.28 km^2 in area. The nodes of the road network are enumerated from *A* to *J* in Fig. 2(a). The edges in the network are all bidirectional, which means that the traffic can move in both the forward and reverse directions for all of the considered road segments.

Although the road network can be described as a primal graph, this study considers the dual graph representation of the road network shown in Fig. 2(b), to mathematically represent the road network using Markov chains. Compared with the primal graph, the connecting roads are represented as nodes in the dual representation. For example, the nodes of the dual graph are named *XY* indicating that *XY* is the road connecting junctions *X* and *Y*, where *X* and *Y* are considered nodes in the primal graph. The dual graph is used to represent the urban road network because it does not depend on the availability of geographic space and has scale-free behavior in urban networks [47]. Compared with the primal representation (Fig. 2(a)), the dual graph clearly shows the relationships between road segments. A detailed explanation on the advantages of using the dual graph representation will be provided in Section 3.1.

The Markov-chain transition matrix can be obtained from the dual graph (Fig. 2(b)). To obtain the transition matrix, the average travel time and the turning probabilities are collected from the actual road segments. Once the travel times are calculated for all road segments, the diagonal components of the transition matrix (i.e., p_{ii}) are calculated using the normalized travel-time values [30]:

$$p_{ii} = \frac{t_i - 1}{t_i}, \quad (i = 1, \ldots, n), \tag{3}$$

where n is the total number of road segments, and t_i is the average travel time for the road segment at node i, which will be explained in Section 3.2. The off-diagonal components of the transition matrix (i.e., p_{ij}) are obtained using the diagonal element in (3) and the turning probability [30]:

$$p_{ij} = (1 - p_{ii}) \cdot tp_{ij}, \quad i \neq j, \tag{4}$$

where tp_{ij} is the turning probability of going from the road segment at node i to the road segment at node j, which will be described in Section 3.2. While the state-transition matrix that characterizes the

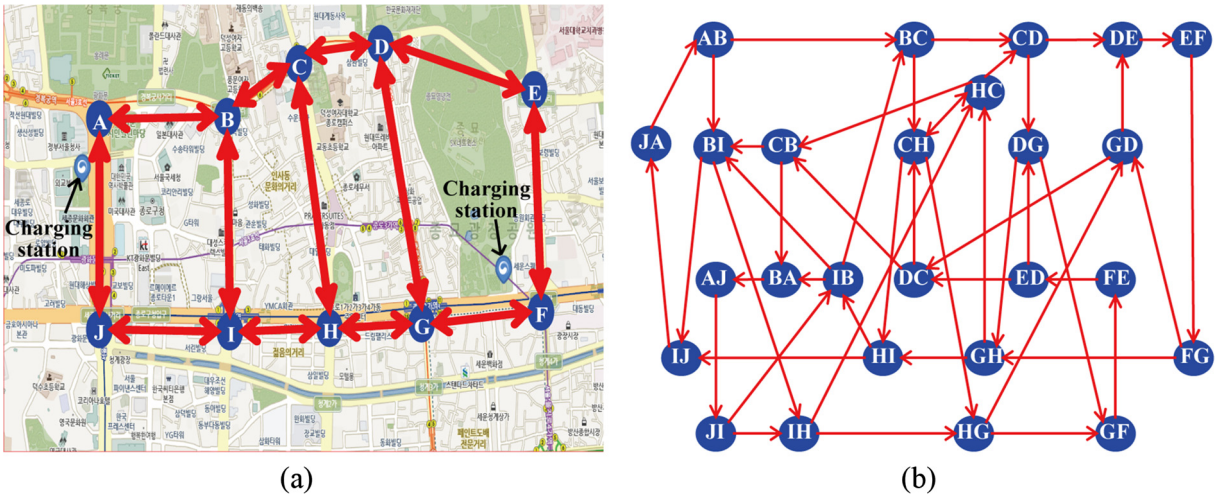

Fig. 2. Considered urban road network with two charging stations. (a) Primal graph representation. (b) Dual graph representation.

traffic flow of the considered urban road network can be constructed using Eqs. (3) and (4), this study applies an additional process, known as the teleportation approach [48–50], to achieve a more accurate prediction of the traffic-flow information in urban areas.

2.3. Markov chain and teleportation approach

As observed in [30], the vehicular density of each road during a sufficiently long period is closely related to the stationary distribution. In a Markov-chain approach, the stationary distribution is actually the left-Perron eigenvector, which is used to describe the vehicular density of the road network. While computing the left-Perron eigenvector of the calculated state-transition matrix using Eqs. (3) and (4) has been reported as an approach for vehicular density prediction [30], such an approach could be subject to prediction-accuracy issues for road networks in urban areas [48]. The most apparent limitation of such a prediction approach is that the assumption of traffic-flow conservation may not be valid for realistic urban traffic networks [48]. In this study, the teleportation approach is used to apply a more reasonable conservation assumption for predicting the traffic flow in urban areas [48–50].

In the teleportation approach, the probabilities that each road segment could be either an origin or a destination are also explicitly considered. These probabilities represent the concept that the road segment is where a vehicle can enter or leave, which may influence the vehicular density at the road segment. The teleportation approach uses a teleportation transition matrix (i.e., $\tilde{\mathbf{U}}$) [48]:

$$\tilde{\mathbf{U}} = \mathbf{P} + \boldsymbol{d}\tilde{\boldsymbol{o}}^T, \tag{5}$$

where $\tilde{\boldsymbol{o}} = \boldsymbol{o}/\|\boldsymbol{o}\|_1$, $\mathbf{P}$ is the transition matrix, $\boldsymbol{o}$ is the probability vector whose elements represent the probability that the corresponding road segment is the origin of a route, and $\boldsymbol{d}$ is the probability vector whose individual elements represent that the corresponding road segment is the destination of a route. While $\mathbf{P}$, the first term on the right side of Eq. (5), is the result of applying the process of Section 2.2, the second term has been introduced to reflect the unique characteristics of urban road networks [48]. To make the teleportation transition matrix, $\tilde{\mathbf{U}}$, stochastic, the scaling method is applied to $\tilde{\mathbf{U}}$ [48]:

$$\mathbf{U} = F\tilde{\mathbf{U}}, \tag{6}$$

where $\mathbf{U}$ is a scaled teleportation transition matrix, and $F = \mathrm{diag}(f_1,\ldots f_n)$ with

$$f_i = \left(\sum_{j=1}^{n} p_{ij} + d_i\left(\sum_{j=1}^{n}\tilde{o}_j\right)\right)^{-1} = \left(\sum_{j=1}^{n} p_{ij} + d_i\right)^{-1}, \tag{7}$$

where f_i is the diagonal element, p_{ij} is the transition matrix, o_i is the origin probability, and d_i is the destination probability. In this study, the scaled teleportation transition matrix, $\mathbf{U}$, is used to determine the vehicular density at each road segment. Once the vehicular density is calculated using $\mathbf{U}$, the arrival rates of vehicles at the charging stations can be determined.

3. Model formulation

3.1. Road network model

In this study, a road network inside the metropolitan area of Seoul, South Korea was considered as shown in Fig. 2(a). While the urban road network of Fig. 2(a) was considered in this study, the proposed analysis approach can also be applied to a larger scope without scalability issues. As shown in Fig. 2(a), the considered road network currently has two charging stations, located near roads *AJ* and *FG*, respectively [3]. This road network was chosen to predict the EV charging-power demand on the two charging stations located in the chosen area.

The dual graph shown in Fig. 2(b) was used to determine the transition matrix. The dual representation of the urban traffic network was used in this study because this representation focuses on the connectivity of the roads and is useful for determining the transition matrix. As introduced in the previous section, the dual graph representation provides more detailed insights about the actual traffic flow (i.e., possible movement directions) compared with the primal graph representation. As an example, the case of traffic flow between node *A* and node *B* can be considered. While it seems possible to go from node *A* to node *B* and then directly move backwards in the primal graph (i.e., Fig. 2(a)), the fact that there is no direct path from road segment *AB* to *BA* in the dual graph implies that such a direct backward movement is not possible at the considered road segment. Examples of causes that restrict such traffic movements include management policies of traffic law enforcement (e.g., prohibiting U-turns) or physical constraints caused by public facilities (e.g., bus stations located in the center of the road). As a result, in case of the road network of Fig. 2, a longer route should be taken to enter road segment *BA* from road segment *AB* as shown in Fig. 2(b).

The size of the transition matrix can also be determined using the dual graph. Ten junctions and 13 bidirectional road segments connecting the junctions are in the primal graph in Fig. 2(a). However, in the dual graph shown in Fig. 2(b), 26 nodes represent the road segments in the primal graph. The number of road segments (i.e., nodes) from the dual graph represents the size of the transition matrix. Therefore, the dual graph shown in Fig. 2(b) can be represented by a 26×26 transition matrix.

3.2. Markov-chain urban traffic model

The arrival rate of EVs at the charging stations can be obtained using the transition matrix and the teleportation transition matrix described in Section 2.

As discussed in Section 2, the transition matrix is determined using the average travel time and the turning probability. To determine the diagonal elements of the transition matrix, the average travel time is calculated using the length of each road segment and the average speed of the road segment:

$$t_i = \frac{l_i}{v_i}, \tag{8}$$

where t_i is the average travel time for the road segment at node i, and v_i is the average speed of the road segment at node i. In this study, the length of each road segment and the average speed on a road segment were determined from actual data provided by the Seoul Transport Operation and Information Service (TOPIS) [51].

It is worth noting that the diagonal components of the transition matrix are zero. This matrix feature originates from the fact that turning around to the same road segment is unlikely to occur, as shown in the dual graph in Fig. 2(b). The turning probability, which is also required to construct the transition matrix as shown in Eq. (4), was also determined using the dual graph. The turning probability is the ratio between the number of vehicles that go through node i to node j and the total number of vehicles that go through node i [52]:

$$tp_{ij} = \frac{N_{ij}}{\sum_{k\in S_i} N_{ik}}, \tag{9}$$

where N_{ij} is the number of vehicles that move from node i to node j, k is the number of nodes connected to node i, and N_{ik} is the number

of vehicles that pass through node *i*. The number of vehicles is determined by counting the number of vehicles passing each road segment and the number of vehicles turning to another road segment. The gathered data were then averaged to calculate the mean probabilities.

In this study, the data were collected from the CCTV provided by TOPIS [51] during three time ranges (i.e., morning, afternoon, and evening). The morning time range is from 7:00 to 9:00, when people are going to work or to school. The afternoon time range is from 12:00 to 14:00, when people are going out to have lunch. The evening time range is from 17:00 to 19:00, when people are heading back to their homes or to other places for personal agendas. These time ranges were chosen to account for vehicles that cannot reach their destinations with the current SOC battery level. During the morning range, it is expected that EVs that were not charged at private facilities overnight (e.g., slow charging performed in the garage) would need to charge the batteries so the vehicles could reach their destinations. The charging-power demand during the afternoon and evening time ranges would mostly come from EVs that could not charge at their workplace, such that the remaining available SOC values were not high enough to drive to their destinations. The time data and vehicle data collected from the real-time CCTV provided by TOPIS [51] were used in this study. During each time range, the number of vehicles was determined by counting the number of vehicles passing each road segment and the number of vehicles turning to another road segment for every 10 min. These gathered data were averaged to determine the turning probability on each time range.

Since the traffic flows for each time period would differ, three transition matrices were obtained overall (i.e., one matrix for each time period). The transition matrix in the morning time range (i.e., $\mathbf{P_m}$) is given by (10). The transition matrices in the afternoon and in the evening time ranges are described in Eqs. (A.1) and (A.2) (i.e., $\mathbf{P_a}$ and $\mathbf{P_e}$), respectively, and are included in Appendix A. The size of each transition matrix would be 26×26, representing the 26 nodes (i.e., road segments) shown in Fig. 2(b) and are taken in alphabetical order. It was observed that the diagonal elements are zeros, which explains that there are no turnarounds on the road network. The elements with 1 show that only one road segment is available from the particular road segment. Elements with values less than 1 indicate that more than one road segment is connected with the particular road segment.

$$\mathbf{P_m} = \begin{bmatrix}
0 & 0 & 0 & 0.2 & 0.8 & 0 & 0 & 0 & 0 & 0 & 0 & 0 & 0 & 0 & 0 & 0 & 0 & 0 & 0 & 0 & 0 & 0 & 0 & 0 & 0 \\
0 & 0 & 0 & 0 & 0 & 0 & 0 & 0 & 0 & 0 & 0 & 0 & 0 & 0 & 0 & 0 & 0 & 0 & 0 & 0 & 0 & 0 & 0 & 0 & 1 \\
0 & 1 & 0 & 0 & 0 & 0 & 0 & 0 & 0 & 0 & 0 & 0 & 0 & 0 & 0 & 0 & 0 & 0 & 0 & 0 & 0 & 0 & 0 & 0 & 0 \\
0 & 0 & 0 & 0 & 0 & 0 & 0.9 & 0.1 & 0 & 0 & 0 & 0 & 0 & 0 & 0 & 0 & 0 & 0 & 0 & 0 & 0 & 0 & 0 & 0 & 0 \\
0 & 0 & 0 & 0 & 0 & 0 & 0 & 0 & 0 & 0 & 0 & 0 & 0 & 0 & 0 & 0 & 0 & 0 & 0 & 0 & 0 & 0.5 & 0.5 & 0 & 0 \\
0 & 0 & 0.9 & 0 & 0.1 & 0 & 0 & 0 & 0 & 0 & 0 & 0 & 0 & 0 & 0 & 0 & 0 & 0 & 0 & 0 & 0 & 0 & 0 & 0 & 0 \\
0 & 0 & 0 & 0 & 0 & 0 & 0 & 0 & 0 & 0.9 & 0.1 & 0 & 0 & 0 & 0 & 0 & 0 & 0 & 0 & 0 & 0 & 0 & 0 & 0 & 0 \\
0 & 0 & 0 & 0 & 0 & 0 & 0 & 0 & 0 & 0 & 0 & 0 & 0 & 0 & 0 & 0 & 0 & 0 & 0.1 & 0.9 & 0 & 0 & 0 & 0 & 0 \\
0 & 0 & 0 & 0 & 0 & 1 & 0 & 0 & 0 & 0 & 0 & 0 & 0 & 0 & 0 & 0 & 0 & 0 & 0 & 0 & 0 & 0 & 0 & 0 & 0 \\
0 & 0 & 0 & 0 & 0 & 0 & 0 & 0 & 0 & 0 & 0 & 0 & 1 & 0 & 0 & 0 & 0 & 0 & 0 & 0 & 0 & 0 & 0 & 0 & 0 \\
0 & 0 & 0 & 0 & 0 & 0 & 0 & 0 & 0 & 0 & 0 & 0 & 0 & 0 & 0 & 0 & 0.5 & 0.5 & 0 & 0 & 0 & 0 & 0 & 0 & 0 \\
0 & 0 & 0 & 0 & 0 & 0 & 0 & 0 & 0.8 & 0 & 0.2 & 0 & 0 & 0 & 0 & 0 & 0 & 0 & 0 & 0 & 0 & 0 & 0 & 0 & 0 \\
0 & 0 & 0 & 0 & 0 & 0 & 0 & 0 & 0 & 0 & 0 & 0 & 0 & 0 & 1 & 0 & 0 & 0 & 0 & 0 & 0 & 0 & 0 & 0 & 0 \\
0 & 0 & 0 & 0 & 0 & 0 & 0 & 0 & 0 & 0 & 0 & 1 & 0 & 0 & 0 & 0 & 0 & 0 & 0 & 0 & 0 & 0 & 0 & 0 & 0 \\
0 & 0 & 0 & 0 & 0 & 0 & 0 & 0 & 0 & 0 & 0 & 0 & 0 & 0 & 0 & 0.1 & 0 & 0.9 & 0 & 0 & 0 & 0 & 0 & 0 & 0 \\
0 & 0 & 0 & 0 & 0 & 0 & 0 & 0 & 0.5 & 0.5 & 0 & 0 & 0 & 0 & 0 & 0 & 0 & 0 & 0 & 0 & 0 & 0 & 0 & 0 & 0 \\
0 & 0 & 0 & 0 & 0 & 0 & 0 & 0 & 0 & 0 & 0 & 0 & 0 & 1 & 0 & 0 & 0 & 0 & 0 & 0 & 0 & 0 & 0 & 0 & 0 \\
0 & 0 & 0 & 0 & 0 & 0 & 0 & 0 & 0 & 0 & 0 & 0 & 0 & 0 & 0 & 0 & 0 & 0 & 0.1 & 0 & 0.9 & 0 & 0 & 0 & 0 \\
0 & 0 & 0 & 0 & 0 & 0.45 & 0.45 & 0.1 & 0 & 0 & 0 & 0 & 0 & 0 & 0 & 0 & 0 & 0 & 0 & 0 & 0 & 0 & 0 & 0 & 0 \\
0 & 0 & 0 & 0 & 0 & 0 & 0 & 0 & 0 & 0 & 0 & 0 & 0 & 0 & 0 & 0.5 & 0.5 & 0 & 0 & 0 & 0 & 0 & 0 & 0 & 0 \\
0 & 0 & 0 & 0 & 0 & 0 & 0 & 0 & 0 & 0 & 0 & 0 & 0 & 0 & 0 & 0 & 0 & 0 & 0 & 0 & 0 & 0.2 & 0 & 0.8 & 0 \\
0 & 0 & 0.9 & 0.1 & 0 & 0 & 0 & 0 & 0 & 0 & 0 & 0 & 0 & 0 & 0 & 0 & 0 & 0 & 0 & 0 & 0 & 0 & 0 & 0 & 0 \\
0 & 0 & 0 & 0 & 0 & 0 & 0 & 0 & 0 & 0 & 0 & 0 & 0 & 0 & 0 & 0 & 0 & 0 & 0.1 & 0.9 & 0 & 0 & 0 & 0 & 0 \\
0 & 0 & 0 & 0 & 0 & 0 & 0 & 0 & 0 & 0 & 0 & 0 & 0 & 0 & 0 & 0 & 0 & 0 & 0 & 0 & 0 & 0 & 0 & 1 & 0 \\
1 & 0 & 0 & 0 & 0 & 0 & 0 & 0 & 0 & 0 & 0 & 0 & 0 & 0 & 0 & 0 & 0 & 0 & 0 & 0 & 0 & 0 & 0 & 0 & 0 \\
0 & 0 & 0 & 0 & 0 & 0 & 0 & 0 & 0 & 0 & 0 & 0 & 0 & 0 & 0 & 0 & 0 & 0 & 0 & 0 & 0 & 0.2 & 0.8 & 0 & 0
\end{bmatrix} \tag{10}$$

The teleportation transition matrix (i.e., $\tilde{\mathbf{U}}$) was determined using the transition matrix stated above (i.e., Eq. (10)) and the probabilities that each road segment could either be an origin or a destination of a route. A uniform distribution was estimated to describe the origin and destination probabilities. Since it was assumed that all road segments could either be the origin or the destination of a route, with 26 nodes in the given road network, the origin and destination probabilities are given respectively as:

$$o_i = 1/26, \text{ and} \tag{11}$$

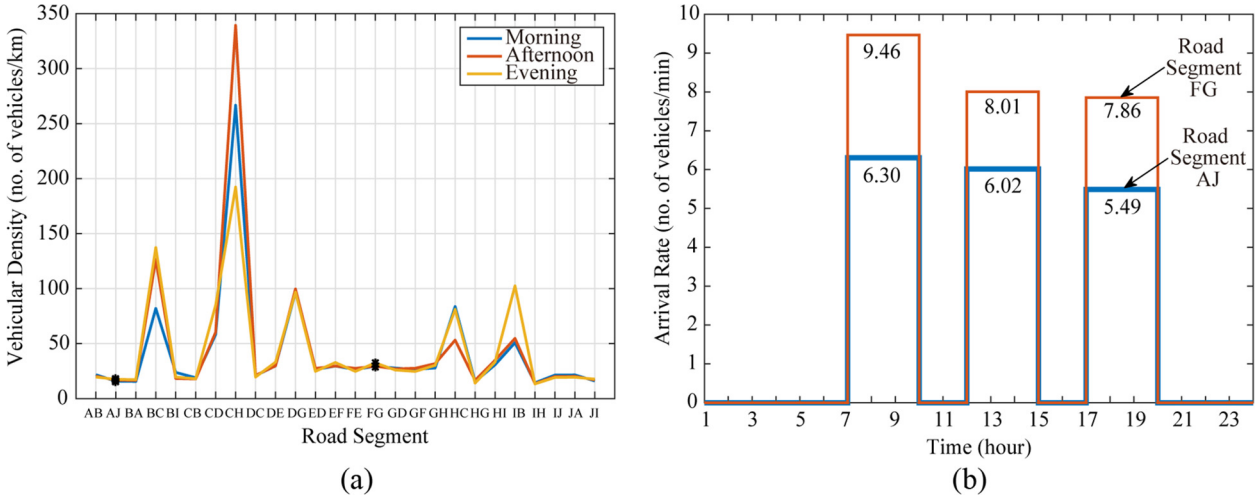

Fig. 3. Markov-chain traffic model result. (a) Vehicular density for every road segment. (b) Arrival rates of vehicles at road segments *AJ* and *FG*.

$$d_i = 1/26, \tag{12}$$

where o_i is the probability that the road segment at node i is the origin of the route, and d_i is the probability that the road segment at node i is the destination of the route. Once the scaled teleportation transition matrix (i.e., **U**) was determined, its stationary distribution (i.e., the left-Perron eigenvector of the scaled teleportation transition matrix) was calculated. The stationary distribution contains the information on the vehicular density of each road segment [30]. That is, the vehicular density (i.e., ρ_i) along a particular road segment at node i is the reciprocal of the computed stationary distribution, which is the mean recurrence time at the road segment at node i [52].

Fig. 3(a) shows the vehicular densities at each road segment in the chosen urban road network for the three considered time ranges (i.e., morning, afternoon, and evening). As depicted, the vehicular density varies on each road segment, and the highest vehicular density can be observed at road segment *CH* for all three time periods. The variation of the vehicular densities over the three time ranges demonstrates that using a single averaged value for estimating the vehicular density does not give accurate values. Not only does the vehicular density value differ depending on the time range, it also shows a large variation over different road segments. Therefore, it is necessary to perform Markov-chain traffic modeling to obtain an accurate estimation.

The vehicular densities at road segments *AJ* and *FG* were used to determine the arrival rates of vehicles at the charging stations on these road segments. As shown in Fig. 3(a), the vehicular densities at road segment *AJ* in the morning, afternoon, and evening time ranges are 15.83 vehicles/km, 16.79 vehicles/km, and 17.51 vehicles/km, respectively. On the other hand, the vehicular densities at road segment *FG* in the morning, afternoon, and evening time ranges are 29.42 vehicles/km, 29.47 vehicles/km, and 32.50 vehicles/km, respectively. In addition, the vehicular density at road segment *FG* is higher than that at road segment *AJ*.

The arrival rate of vehicles at the charging station on each road segment can be determined by the vehicular density and the average speed of the road segment. In other words, the arrival rate of vehicles at the charging station on the i^{th} road segment (i.e., α_i) equals the product of the vehicular density on the i^{th} road segment and its average speed. That is,

$$\alpha_i = \rho_i v_i, \tag{13}$$

where α_i is the arrival rate at the i^{th} road segment, ρ_i is the vehicular density on the i^{th} road segment, and v_i is the mean speed of the i^{th} road segment. The arrival rates of the vehicles at road segments *AJ* and *FG* were calculated using Eq. (13). Fig. 3(b) shows the arrival rates of vehicles at road segments *AJ* and *FG* for the three time ranges. The arrival rate of vehicles at road segment *FG* is higher than that at road segment *AJ*.

3.3. EV charging characteristics

The EV charging-power demand is influenced by various factors, e.g., vehicle type, battery technology, battery capacity, battery SOC, charging-power level, and charging pattern. In this study, these factors were considered to determine the EV charging-power demand at the charging stations.

According to the Electric Vehicle Charging Information System [3], the EVs developed and deployed in South Korea use lithium-ion polymer batteries with different capacities and travel ranges, depending on their types and sizes. In this paper, a Soul EV five-seater medium-size vehicle manufactured by Kia Motors, with a maximum speed of 145 km/h, was used in the simulation [3]. This EV uses a 27-kW h lithium-ion polymer battery that enables a 148-km drive range. Since the battery capacity of the considered EV model is the highest one among the EVs that are deployed in the South Korean market [3], the maximum charging-power demand value could be estimated from the current study.

The remaining available battery state-of-charge (SOC) (i.e., the SOC level of the discharged EV that arrives at the fast-charging station) also has an influence on the EV charging-power demand. In this study, the remaining available battery SOC is a random variable with a Gaussian distribution, of which the probability density function (*pdf*) is defined as [53]:

$$f_{soc}(soc) = \frac{1}{\sigma_{soc}\sqrt{2\pi}} e^{\frac{-(soc-\mu_{soc})^2}{2\sigma_{soc}^2}}, \tag{14}$$

where *soc* is the remaining available battery SOC, μ_{soc} is the average remaining available SOC value, and σ_{soc} is the standard deviation. The remaining available battery SOC was generated by the random sampling of a Gaussian *pdf* with $\mu_{soc} = 0.5$ and $\sigma_{soc} = 0.3$ [53], as shown in Fig. 4(a).

In this study, once the arrival rate of the vehicles at the road segments was determined using the Markov-chain traffic model, the remaining available battery SOC was generated by random sampling. It was also assumed that only vehicles whose remaining available battery SOC level was between or equal to 0.2 and 0.3 would be charged. Vehicles with a remaining available SOC higher

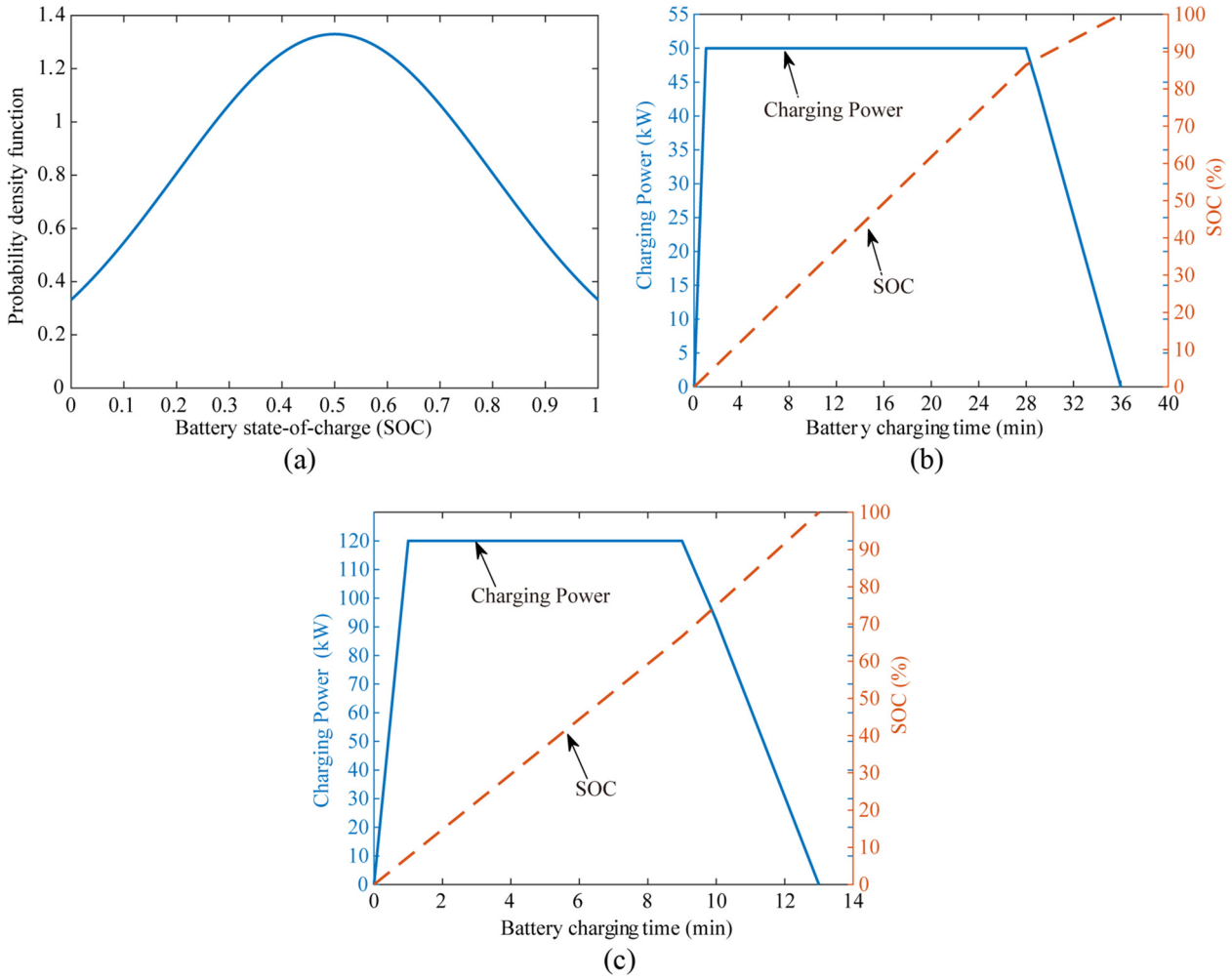

Fig. 4. Battery characteristics. (a) Gaussian distribution of the remaining available battery SOC. (b) Battery-charging profile of a lithium-ion polymer battery with 50-kW charging power. (c) Battery-charging profile of a lithium-ion polymer battery with 120-kW charging power.

than 0.3 would not be charged. Such vehicles would simply drive through the road segments instead of stopping at the charging station for battery charging. (i.e., their remaining available battery SOC is high enough for the EVs to reach their destination without charging.)

The EV charging-power demand was also affected by the charging-power classification. In this study, fast-charging classifications with 50-kW charging power and 120-kW charging power were used. In the simulation, 90% of arriving EVs was assumed to be charged by 50-kW charging power and 10% of arriving EVs was assumed to be charged using 120-kW charging power. The proportions of arriving EVs charged by the specific charging power can be changed based on the number of different fast charging power classes in the investigated area. These proportions were assumed because 50-kW charging power is the major charging power of the rapid chargers available in South Korea [3]. The 120-kW charging system was also considered to reflect the development trend in EV charger systems by competitive EV manufactures [54]. The slow-charging classification is out of the scope of this paper for simplicity of the study and could be investigated in the future work. All the EVs deployed in South Korea use lithium-ion polymer batteries [3]. Therefore, this study used the lithium-ion polymer battery-charging profiles shown in Fig. 4 (b) and (c) with fast-charging classifications based on the simplified piecewise-linear charging profile model used in [55] based on statistical observation. These battery-charging profiles were based on EV battery capacity and the charging power of the rapid chargers used in the study. Fig. 4(b) and (c) show the battery-charging power and related battery SOC profiles for the lithium-ion polymer battery of the Soul EV used in the simulation. As depicted in Fig. 4(b) and (c), 36 min were required to fully charge a lithium-ion polymer battery with a 50-kW rapid charger, and 13 min were required to fully charge a lithium-ion polymer battery with a 120-kW rapid charger respectively.

The charging pattern can also affect the charging-power demand. In this study, the charging pattern is defined as the charging strategy considered by the EV operators. While charging the EV batteries up to the maximum SOC level whenever the EV visits a charging station would be the most simple and intuitive charging pattern, it is also possible that the driver would not follow such a simple charging pattern, and only partially charge at a fast-charging station for several reasons. For example, the relatively expensive service cost of fast charging compared with that of slow charging could force the driver to charge the battery only until it was sufficient to reach the next destination, instead of fully charging the battery.

Since the overall charging-power demand at each charging station would be affected by the actual charging pattern of each EV

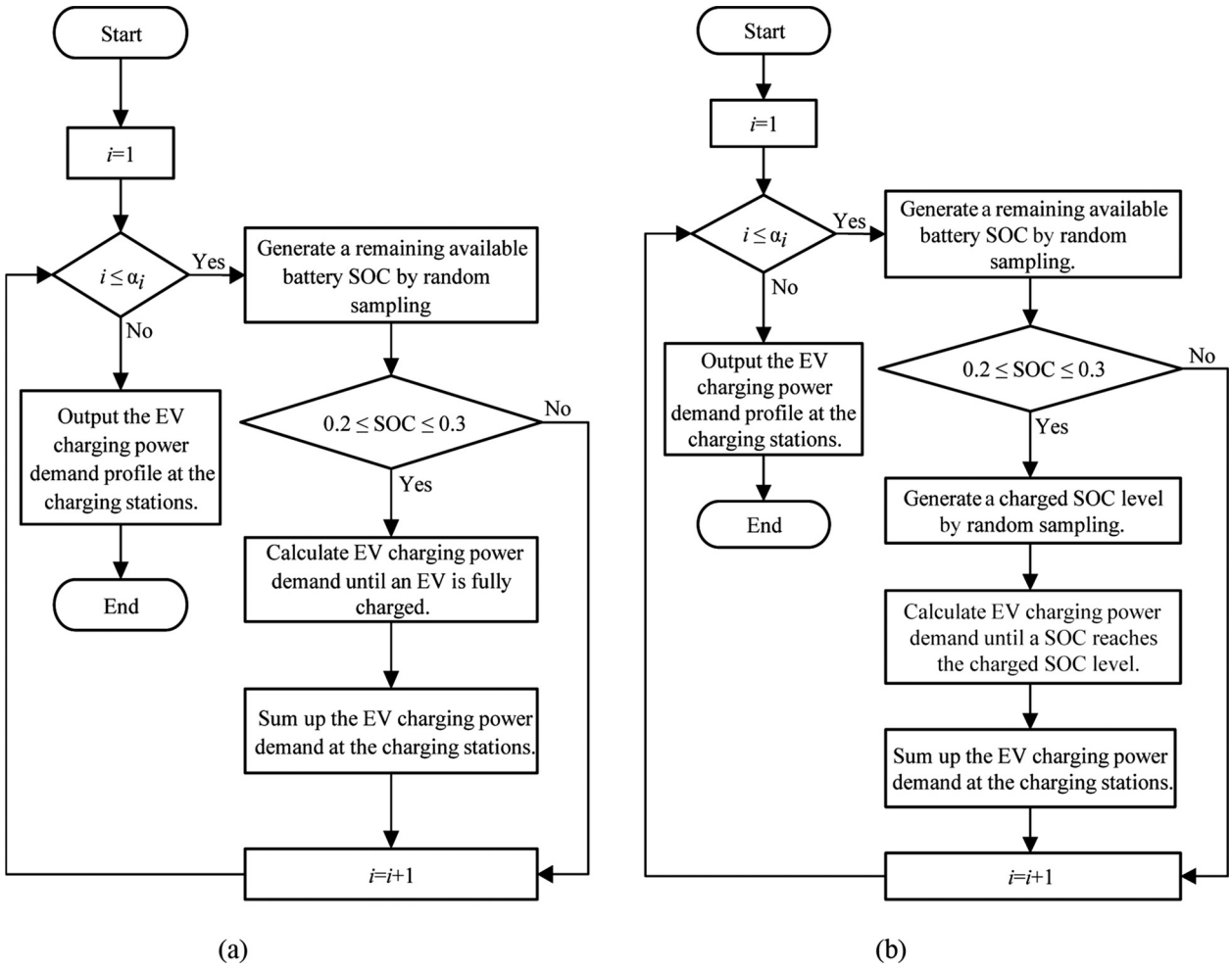

Fig. 5. Flowchart of the proposed EV charging-power demand model. (a) Fully charged. (b) Charged up to a randomly generated SOC level.

driver, it is also necessary to study how the different charging patterns could affect the charging-power demand. To study the effect of different charging patterns, a charged SOC (i.e., the SOC level of an EV after finishing its battery charging at a fast-charging station) is assumed to be a random variable with a Gaussian distribution and depend on the probability density function (*pdf*) defined as:

$$f_c(c) = \frac{1}{\sigma_c\sqrt{2\pi}} e^{\frac{-(c-\mu_c)^2}{2\sigma_c^2}}, \tag{15}$$

where c is the charged SOC value, μ_c is the average charged SOC value, and σ_c is its standard deviation. In this study, the charged SOC is randomly generated with $\mu_c = 0.3$ and $\sigma_c = 0.1$. While other values for the average and standard deviation could be used in (15), such values were assumed as an illustrative example to consider cases that the EV user would not fully but partially charge the battery at public fast-charging stations because of cost or time constraints.

3.4. EV charging-power demand calculation

Fig. 5 shows the flow chart used in this study to estimate the EV charging-power demand. The EV charging-power demand-calculation process uses the information on the arrival rates, the SOC values of the batteries inside the arriving EVs, and the charged SOC value of the batteries inside the EVs that have finished charging.

Once the arrival rate of the EVs on the road segments is obtained based on the Markov-chain traffic model, the values of the remaining available battery SOC levels are generated using random sampling according to (14). If the remaining available battery SOC is between or equal to 0.2 and 0.3, the corresponding vehicle is expected to charge the battery. Accordingly, the charging power of such a vehicle should be considered to estimate the EV charging-power demand. By using the information on the available battery SOC level and the charged SOC level, the charging-power demand for each EV can be calculated by the charging profiles shown in Fig. 4(b) and (c). It is worth noting that the charged SOC level can differ depending on the charging pattern being considered.

In this study, it is assumed that EVs would either be fully charged (i.e., Fig. 5(a)) or charged up to the random SOC values generated by the *pdf* of Eq. (15) (i.e., Fig. 5(b)). To obtain the overall EV charging-power demand, the charging-power demand of each EV is calculated until the number of EVs that have visited the charging station reaches the predicted value of vehicles arriving at the charging station. Once this number is reached, the overall charging-power demand can be found by summing the discretized charging-power demand for all of the considered vehicles. In other words, the EV charging-power demand at the charging station located on the i^{th} road segment at time t can be estimated as:

$$P_i(t) = \sum_{i=1}^{\alpha_i} P_d(t), \tag{16}$$

where $P_i(t)$ is the total EV charging-power demand at time t, α_i is the number of discharged EVs arriving at the charging station on the i^{th} road segment at time t, and $P_d(t)$ is the charging power of each charger at the charging station on the i^{th} road segment at time t.

It is worth noting that the charging system can be viewed as an example of a queueing system (i.e., charging system with EVs forming a queue) for which the stability condition that originates from the M/M/s queueing theory can be derived [24,56]. In this paper, the following conditions were assumed at the charging-station road segments:

(i) The arrival rate (i.e., α_i) of discharged EVs at the charging stations is based on the Markov-chain traffic model.
(ii) There are s identical chargers in the charging stations located at road segments *AJ* and *FG* of the urban road network.
(iii) The charging-service rate for all chargers equals μ, approximated as the ratio of the average charging power of each charger (i.e., P_d (kW)) and the recharging capacity per vehicle (i.e., *Cap* (kW h)), which is independently and exponentially distributed as described in [24].
(iv) All EVs will be charged by the next available chargers following first-come-first-served rules.
(v) All EVs leave the charging stations directly after charging their batteries.

Under such assumptions, a condition that is linked to the stability of the queueing system can be expressed by considering the occupational rate of the charger (β: the probability that a charger is active) as [24,56]:

$$\beta = \frac{\alpha_i}{s\mu} < 1, \tag{17}$$

where α_i is the arrival rate of discharged EVs, s is the number of identical chargers, and μ is the charging service rate of the chargers. The inequality condition of (17) can be rewritten to derive the minimum number of chargers that are required to ensure the stability of the queueing system:

$$s > \frac{\alpha_i}{\mu}. \tag{18}$$

In the case of this paper, such an equality condition means that the system will be considered stable as long as the charging stations can handle the arrival of discharged EVs and the queue of discharged EVs does not build up to infinity.

4. Numerical examples

This section provides numerical examples to describe the time-spatial EV charging-power demand model based on the Markov-chain traffic model and the charging-power demand calculation approach presented in Section 3.

Different from previous studies [14,24–26], this study used the real-time CCTV data at the junctions of each road segment in the chosen road network (i.e., Fig. 2(a)) in South Korea for the simulation to show more realistic results. Compared with most previous research works [5–7] which considered private charging locations and fixed charging-start times, the speed and the number of vehicles passing through the road segments were collected for the three time ranges (i.e., morning, afternoon, and evening) at each road segment. The number of discharged EVs arriving at the charging stations was determined by the EV arrival rate at each road segment using the collected real-time CCTV data at each time range. The charging-power demand load profiles were calculated based on the following assumptions:

(1) Discharged EVs are defined as EVs whose remaining available battery SOC is between or equal to 0.2 and 0.3, and only these EVs would be charged at the charging stations;
(2) The remaining available battery SOC of the EVs arriving at the charging stations was generated using random sampling;
(3) Both charging stations in the chosen area shown in Fig. 2(a) were equipped with 50-kW fast chargers and 120-kW fast chargers; and
(4) 90% of arriving discharged EVs was charged with 50-kW charging power, and 10% of the arriving discharged EVs was charged with 120-kW charging power.

Considering that the battery of each EV can be charged to a different SOC level, depending on the operation patterns and drive conditions, this study investigated the following four charging scenarios. In the first scenario, all of the discharged vehicles will be fully charged at the charging station. In the second scenario, the batteries of the discharged EVs will be charged so that the SOC level of the charged EVs will follow the Gaussian distribution, as in Eq. (15). In the third scenario, only 10% of the discharged vehicles will be fully charged and 90% of the vehicles will be charged according to the SOC values randomly generated using Eq. (15). The fourth scenario is similar to the third approach, increases the ratio of fully charged vehicles from 10% to 20% and decreases the ratio of randomly charged vehicles from 90% to 80%.

Figs. 6 and 7 show the EV charging-power demand load profiles at the two charging stations located at road segments *AJ* and *FG*, respectively. As depicted in the figures, the charging-power demand at each charging station shows three charging periods. They represent the morning, afternoon, and evening time ranges in which EVs must be charged in order to reach their destinations because the EV owners could not charge their EVs at home or at work. The charging-power demand at the charging station on road segment *FG* (i.e., Fig. 7) is higher than the charging-power demand at the charging station on road segment *AJ* (i.e., Fig. 6) because the arrival rate (i.e., Fig. 3(b)) of the vehicles at road segment *FG* is higher than that at road segment *AJ*.

Fig. 6 shows the EV charging-power demand profile at the charging station located on road segment *AJ*. As shown in Fig. 3(b), the arrival rates of EVs on road segment *AJ* in the morning, afternoon, and evening time ranges are respectively 6.30, 6.02, and 5.49 vehicles per minute. Accordingly, the highest charging-power demand in the morning and afternoon charging periods is almost the same, and is higher than the charging-power demand in the evening.

Fig. 6(a) shows the EV charging-power demand of the charging station located on road segment *AJ* when all the discharged EVs arriving at the charging station were fully charged. This case (i.e., Fig. 6(a)) shows the highest EV charging-power demand among all the charging scenarios. Fig. 6(b), in which the randomly charged SOCs are considered, shows the lowest EV charging-power demand. Fig. 6(c) and (d) show the EV charging-power demand of the combination of the first two scenarios. Fig. 6(c) illustrates the EV charging-power demand of the combination where 10% of the discharged EVs were fully charged and 90% of the discharged EVs were charged with a randomly charged SOC. Fig. 6(d) shows the EV charging-power demand of the combination where 20% of the discharged EVs were fully charged and 80% of the discharged EVs were charged to a random SOC level. The EV charging-power demand of these two combinations is almost the same as that

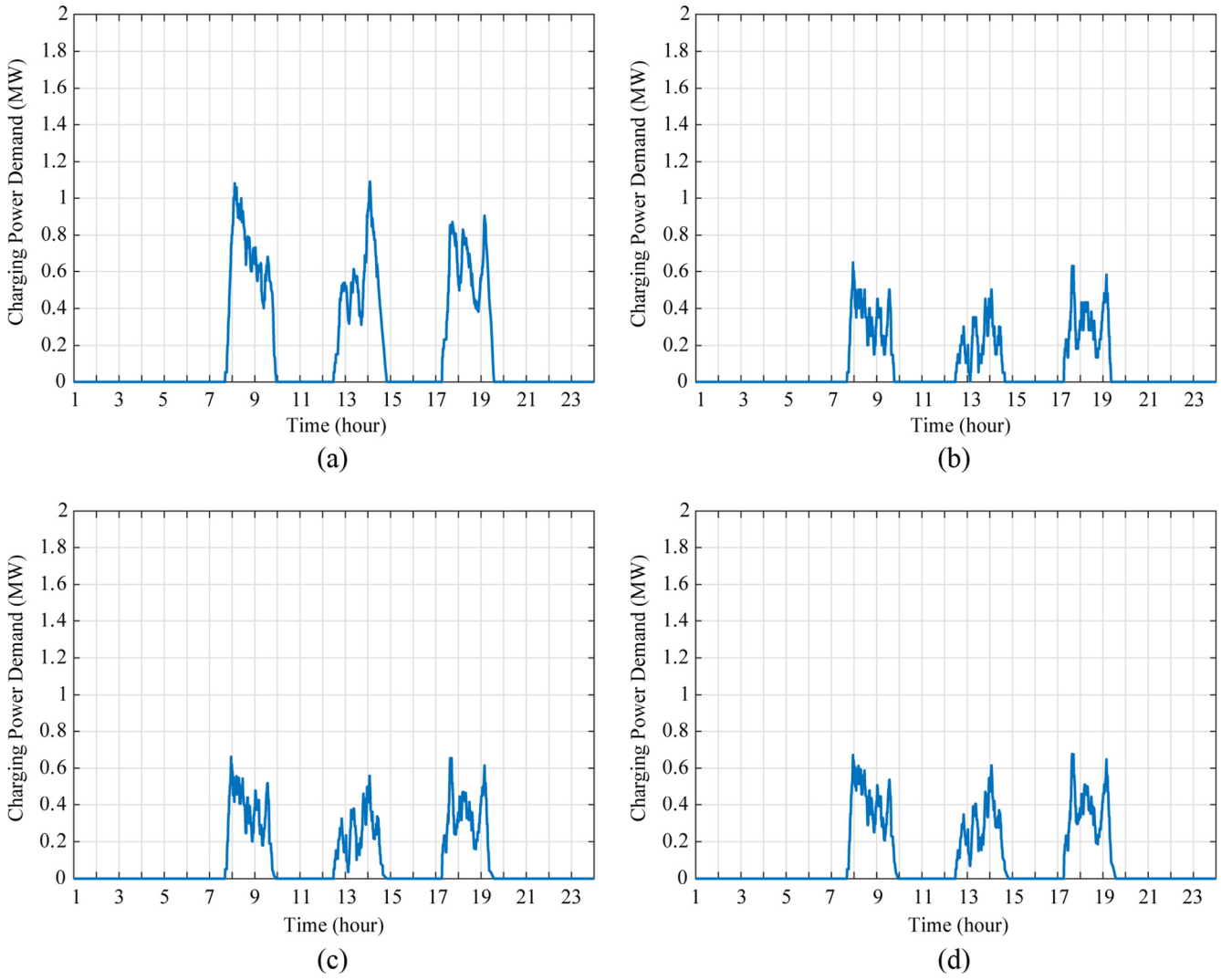

Fig. 6. EV charging-power demand profile at the charging station on road segment *AJ*. (a) 100% fully-charged. (b) 100% random SOC. (c) 10% fully-charged and 90% random SOC. (d) 20% fully-charged and 80% random SOC.

shown in Fig. 6(c) and (d). The maximum values in Fig. 6(c) are 0.6618, 0.5591, and 0.6550 while in Fig. 6(d), the maximum values are 0.6718, 0.6157, and 0.6772 for morning, afternoon, and evening time ranges respectively. The mean values in Fig. 6(c) are 0.3381, 0.2272, and 0.3143 while in Fig. 6(d), 0.3707, 0.2567, and 0.3420 are the mean values for each time range, respectively. Since more vehicles are commanded to be fully charged in Fig. 6(c), the maximum and the mean values of the charging-power demand in Fig. 6(d) are larger than those in Fig. 6(c).

Fig. 7 shows the EV charging-power demand profile for the charging station located on road segment *FG* for the three charging periods and four charging scenarios. The arrival rates of the EVs at road segment *FG* are 9.46, 8.01, and 7.86 vehicles per minute in the morning, afternoon, and evening, respectively, as shown in Fig. 3 (b). Similar to Fig. 6, Fig. 7(a) shows the highest EV charging-power demand among the four scenarios because all the discharged EVs arriving at the charging station in this case were fully charged.

On the other hand, Fig. 7(b) shows the lowest EV charging-power demand among the four operation scenarios, because the discharged EVs were charged to a random SOC level. Fig. 7 (c) and (d) show the EV charging-power demand of the combination of the first two scenarios. Fig. 7(c) shows the EV charging-power demand when 10% of the discharged EVs were fully charged and 90% of the discharged EVs charged their batteries to a random SOC. Fig. 7(d) depicts the EV charging-power demand when 20% of the discharged EVs were fully charged and 80% of the discharged EVs charged their batteries to a random SOC. Fig. 7(c) and (d) show almost the same EV charging-power demand. The maximum values of each time range in Fig. 7(c) are 0.9505, 0.6959, and 0.6303 respectively while in Fig. 7(d), the maximum values are 1.0220, 0.7409, and 0.6653 for morning, afternoon, and evening time ranges respectively. The mean values in Fig. 7(c) are 0.5113, 0.3683, and 0.3711 while in Fig. 7(d), the mean values are 0.5679, 0.4107, and 0.4043 for the morning, afternoon, and evening time ranges respectively. The maximum values and mean values in Fig. 7(d) show higher values compared to the maximum values and mean values in Fig. 7(c).

As can be seen in Figs. 6 and 7, the maximum charging-power demand value at the charging station on road segment *FG* for each charging period is larger than that at the charging station on road segment *AJ*. This can be explained by the larger arrival rate at the

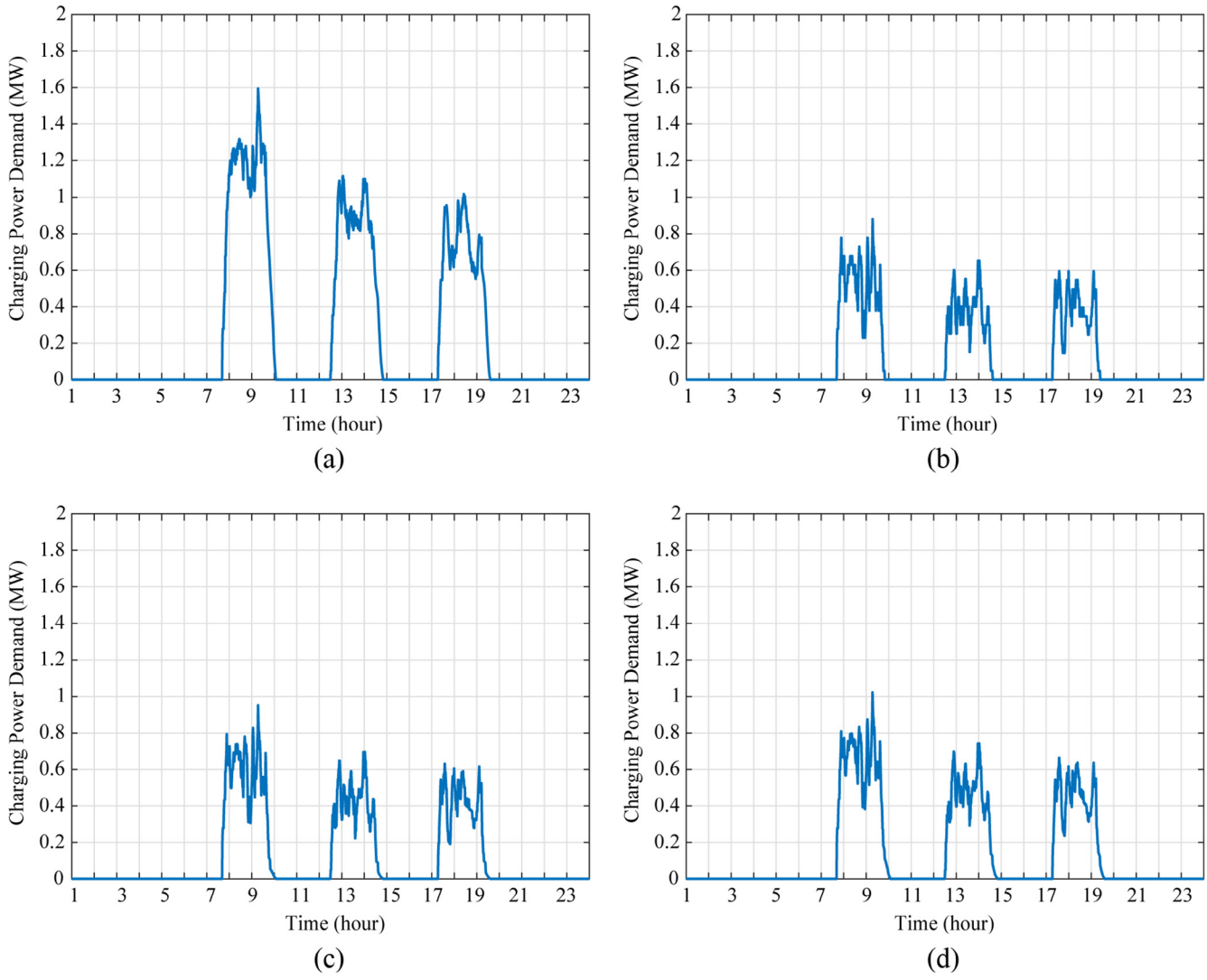

Fig. 7. EV charging-power demand profile at the charging station at road segment *FG*. (a) 100% fully-charged. (b) 100% random SOC. (c) 10% fully-charged and 90% random SOC. (d) 20% fully-charged and 80% random SOC.

Table 1
Comparison of EV charging-power demand for different scenarios at the charging station at road segment *AJ*.

Scenario	Max. Charging-Power Demand (MW)			Mean Charging-Power Demand (MW)		
	M	A	E	M	A	E
1	1.0799	1.0900	0.9047	0.6316	0.4930	0.5634
2	0.6518	0.5025	0.6328	0.3055	0.1977	0.2866
3	0.6618	0.5591	0.6550	0.3381	0.2272	0.3143
4	0.6718	0.6157	0.6772	0.3707	0.2567	0.3420
5	0.6818	0.6722	0.6994	0.4033	0.2863	0.3697
6	0.7243	0.7288	0.7216	0.4359	0.3158	0.3973

1 = 100% fully-charged, 2 = 100% random SOC, 3 = 10% fully-charged and 90% random SOC, 4 = 20% fully-charged and 80% random SOC, 5 = 30% fully-charged and 70% random SOC, 6 = 40% fully-charged and 60% random SOC, M = morning, A = afternoon, and E = evening.

road segment *FG* charging station than that of road segment *AJ*, as shown in Fig. 3(b). In addition, the difference in the charging-power demand between the afternoon period and the evening period is relatively smaller in Fig. 7 compared with Fig. 6. Such an observation could be explained by the fact that the vehicular density variation is smaller in road segment *FG* than that in segment *AJ*. Such observations show that the EV charging-power demand characteristics for urban areas should be predicted comprehensively in terms of charging location and time periods. The effect of locations and time periods should not be overlooked when expecting reasonable prediction results of the EV charging-power demand.

To study how the change in charging patterns affects the charging-power demand, the maximum and mean values of the EV charging-power demand of six cases are shown in Tables 1 and 2. The results of two additional operation scenarios (i.e., Sce-

Table 2
Comparison of EV charging-power demand for different scenarios at the road segment *FG* charging station.

Scenario	Max. Charging-Power Demand (MW)			Mean Charging-Power Demand (MW)		
	M	A	E	M	A	E
1	1.5945	1.1165	1.0172	1.0210	0.7498	0.6702
2	0.8789	0.6509	0.5953	0.4547	0.3259	0.3378
3	0.9505	0.6959	0.6303	0.5113	0.3683	0.3711
4	1.0220	0.7409	0.6653	0.5679	0.4107	0.4043
5	1.0936	0.7859	0.7003	0.6246	0.4531	0.4375
6	1.1652	0.8309	0.7353	0.6812	0.4955	0.4708

1 = 100% fully-charged, 2 = 100% random SOC, 3 = 10% fully-charged and 90% random SOC, 4 = 20% fully-charged and 80% random SOC, 5 = 30% fully-charged and 70% random SOC, 6 = 40% fully-charged and 60% random SOC, M = morning, A = afternoon, and E = evening.

nario 5 and Scenario 6) were added to the tables. In Scenario 5, only 30% of the discharged vehicles are fully charged and 70% of the discharged vehicles are charged to a random SOC. In Scenario 6, 40% of the discharged vehicles are fully charged and 60% of the discharged vehicles are charged to a random SOC.

As depicted in Tables 1 and 2, Scenario 1 (i.e., all vehicles are fully charged) shows the highest maximum and mean EV charging-power demand, while Scenario 2 (i.e., all vehicles are charged according to a random charging profile) shows the lowest maximum and mean EV charging-power demand. In addition, there is no abrupt change in the EV charging-power demand when the ratio of vehicles being fully charged to the vehicles being randomly charged varies, as shown in Scenarios 3, 4, 5, and 6. By comparing the data shown in Table 2, it is worth noting that the mean charging-power demand of Scenario 1 could be over 2.5 times larger than that of Scenario 2. Such a comparison result demonstrates that the SOC charging profile can significantly affect the load demand in an electric network with high EV utilization. In addition, the charging-power demand increases as the ratio of vehicles that are being fully charged increases. Such a trend can be observed by comparing the results of Scenarios 3, 4, 5, and 6. From a power-network management perspective, the variation in the load demand caused by different operation scenarios (i.e., charging patterns) demonstrates the importance of considering the effect of different EV charging patterns on the power-system load demand.

5. Conclusion

This paper proposed a time-spatial EV charging-power demand forecast model for urban areas. Once the arrival rates of the discharged EVs at the charging stations were calculated using a Markov-chain-based approach, the EV charging-power demand was calculated using the traffic data (i.e., arrival rate) and EV battery information (i.e., SOC level and charging pattern). To achieve a more realistic and practical prediction result, real-time CCTV data of Seoul, South Korea were used. In addition, the teleportation approach was considered during the traffic-flow modeling process so that the traffic characteristics in urban areas could also be included in the system model.

Numerical examples to predict the EV charging-power demand at the charging stations located on two road segments in an urban area were presented in Section 4. The EV charging-power demand profile at each charging station equipped with fast chargers was studied using the proposed approach. Three charging periods (i.e., morning, afternoon, and evening) were studied. While a higher EV charging-power demand was observed in the charging stations with a higher vehicle arrival rate, the charging-power demand profiles at each charging station were affected by different parameter values. In particular, the charging-power demand profiles were influenced by the number of discharged vehicle arriving at the charging stations, remaining available SOC, charged SOC, and charging rate of the charging infrastructures. The effect of such parameter values on the charging-power demand was demonstrated by a comprehensive simulation that considered six operation scenarios. The highest EV charging-power demand was observed when all discharged vehicles were fully charged, while the lowest EV charging-power demand was observed when all vehicles had a randomly charged SOC. The relatively large difference in charging-power demand between the two charging stations demonstrated that the prediction accuracy of charging-power demand in urban road networks could be improved using comprehensive traffic data that could capture the differences among different charging locations and time periods.

The presented time-spatial model of the EV charging-power demand may allow utility operators to plan distribution systems in future power systems, especially in urban areas. In addition, the time-spatial model can also contribute to deciding on investment and operation plans for adaptive EV charging infrastructures with renewable energy resources and energy storage systems, depending on the EV charging-power demand in urban areas. This paper would also benefit engineers and researchers by providing results that more realistically characterize the EV charging-power demand pattern of urban areas to assess its impact on power systems.

Acknowledgment

This work was supported by the Korea Institute of Energy Technology Evaluation and Planning (KETEP) and the Ministry of Trade, Industry & Energy (MOTIE) of the Republic of Korea (No. 20161210200560).

Appendix A

$$\mathbf{P_a} = \begin{bmatrix}
0 & 0 & 0 & 0.1 & 0.9 & 0 & 0 & 0 & 0 & 0 & 0 & 0 & 0 & 0 & 0 & 0 & 0 & 0 & 0 & 0 & 0 & 0 & 0 & 0 \\
0 & 0 & 0 & 0 & 0 & 0 & 0 & 0 & 0 & 0 & 0 & 0 & 0 & 0 & 0 & 0 & 0 & 0 & 0 & 0 & 0 & 0 & 0 & 1 \\
0 & 1 & 0 & 0 & 0 & 0 & 0 & 0 & 0 & 0 & 0 & 0 & 0 & 0 & 0 & 0 & 0 & 0 & 0 & 0 & 0 & 0 & 0 & 0 \\
0 & 0 & 0 & 0 & 0 & 0 & 0.8 & 0.2 & 0 & 0 & 0 & 0 & 0 & 0 & 0 & 0 & 0 & 0 & 0 & 0 & 0 & 0 & 0 & 0 \\
0 & 0 & 0 & 0 & 0 & 0 & 0 & 0 & 0 & 0 & 0 & 0 & 0 & 0 & 0 & 0 & 0 & 0 & 0 & 0 & 0 & 0.5 & 0.5 & 0 & 0 \\
0 & 0 & 0.8 & 0 & 0.2 & 0 & 0 & 0 & 0 & 0 & 0 & 0 & 0 & 0 & 0 & 0 & 0 & 0 & 0 & 0 & 0 & 0 & 0 & 0 & 0 \\
0 & 0 & 0 & 0 & 0 & 0 & 0 & 0 & 0 & 0.9 & 0.1 & 0 & 0 & 0 & 0 & 0 & 0 & 0 & 0 & 0 & 0 & 0 & 0 & 0 & 0 \\
0 & 0 & 0 & 0 & 0 & 0 & 0 & 0 & 0 & 0 & 0 & 0 & 0 & 0 & 0 & 0 & 0 & 0.1 & 0.9 & 0 & 0 & 0 & 0 & 0 & 0 \\
0 & 0 & 0 & 0 & 0 & 1 & 0 & 0 & 0 & 0 & 0 & 0 & 0 & 0 & 0 & 0 & 0 & 0 & 0 & 0 & 0 & 0 & 0 & 0 & 0 \\
0 & 0 & 0 & 0 & 0 & 0 & 0 & 0 & 0 & 0 & 0 & 0 & 1 & 0 & 0 & 0 & 0 & 0 & 0 & 0 & 0 & 0 & 0 & 0 & 0 \\
0 & 0 & 0 & 0 & 0 & 0 & 0 & 0 & 0 & 0 & 0 & 0 & 0 & 0 & 0 & 0 & 0.6 & 0.4 & 0 & 0 & 0 & 0 & 0 & 0 & 0 \\
0 & 0 & 0 & 0 & 0 & 0 & 0 & 0 & 0.8 & 0 & 0.2 & 0 & 0 & 0 & 0 & 0 & 0 & 0 & 0 & 0 & 0 & 0 & 0 & 0 & 0 \\
0 & 0 & 0 & 0 & 0 & 0 & 0 & 0 & 0 & 0 & 0 & 0 & 0 & 0 & 1 & 0 & 0 & 0 & 0 & 0 & 0 & 0 & 0 & 0 & 0 \\
0 & 0 & 0 & 0 & 0 & 0 & 0 & 0 & 0 & 0 & 0 & 1 & 0 & 0 & 0 & 0 & 0 & 0 & 0 & 0 & 0 & 0 & 0 & 0 & 0 \\
0 & 0 & 0 & 0 & 0 & 0 & 0 & 0 & 0 & 0 & 0 & 0 & 0 & 0 & 0 & 0.2 & 0 & 0.8 & 0 & 0 & 0 & 0 & 0 & 0 & 0 \\
0 & 0 & 0 & 0 & 0 & 0 & 0 & 0 & 0.5 & 0.5 & 0 & 0 & 0 & 0 & 0 & 0 & 0 & 0 & 0 & 0 & 0 & 0 & 0 & 0 & 0 \\
0 & 0 & 0 & 0 & 0 & 0 & 0 & 0 & 0 & 0 & 0 & 0 & 0 & 1 & 0 & 0 & 0 & 0 & 0 & 0 & 0 & 0 & 0 & 0 & 0 \\
0 & 0 & 0 & 0 & 0 & 0 & 0 & 0 & 0 & 0 & 0 & 0 & 0 & 0 & 0 & 0 & 0 & 0.1 & 0 & 0.9 & 0 & 0 & 0 & 0 & 0 \\
0 & 0 & 0 & 0 & 0 & 0.5 & 0.5 & 0 & 0 & 0 & 0 & 0 & 0 & 0 & 0 & 0 & 0 & 0 & 0 & 0 & 0 & 0 & 0 & 0 & 0 \\
0 & 0 & 0 & 0 & 0 & 0 & 0 & 0 & 0 & 0 & 0 & 0 & 0 & 0 & 0 & 0.5 & 0.5 & 0 & 0 & 0 & 0 & 0 & 0 & 0 & 0 \\
0 & 0 & 0 & 0 & 0 & 0 & 0 & 0 & 0 & 0 & 0 & 0 & 0 & 0 & 0 & 0 & 0 & 0 & 0 & 0 & 0.2 & 0 & 0.8 & 0 & 0 \\
0 & 0 & 0.9 & 0.1 & 0 & 0 & 0 & 0 & 0 & 0 & 0 & 0 & 0 & 0 & 0 & 0 & 0 & 0 & 0 & 0 & 0 & 0 & 0 & 0 & 0 \\
0 & 0 & 0 & 0 & 0 & 0 & 0 & 0 & 0 & 0 & 0 & 0 & 0 & 0 & 0 & 0 & 0 & 0 & 0.2 & 0.8 & 0 & 0 & 0 & 0 & 0 \\
0 & 0 & 0 & 0 & 0 & 0 & 0 & 0 & 0 & 0 & 0 & 0 & 0 & 0 & 0 & 0 & 0 & 0 & 0 & 0 & 0 & 0 & 0 & 1 & 0 \\
1 & 0 & 0 & 0 & 0 & 0 & 0 & 0 & 0 & 0 & 0 & 0 & 0 & 0 & 0 & 0 & 0 & 0 & 0 & 0 & 0 & 0 & 0 & 0 & 0 \\
0 & 0 & 0 & 0 & 0 & 0 & 0 & 0 & 0 & 0 & 0 & 0 & 0 & 0 & 0 & 0 & 0 & 0 & 0 & 0 & 0.2 & 0.8 & 0 & 0 & 0
\end{bmatrix}$$

$$\mathbf{P_e} = \begin{bmatrix}
0 & 0 & 0 & 0.1 & 0.9 & 0 & 0 & 0 & 0 & 0 & 0 & 0 & 0 & 0 & 0 & 0 & 0 & 0 & 0 & 0 & 0 & 0 & 0 & 0 & 0 \\
0 & 0 & 0 & 0 & 0 & 0 & 0 & 0 & 0 & 0 & 0 & 0 & 0 & 0 & 0 & 0 & 0 & 0 & 0 & 0 & 0 & 0 & 0 & 1 \\
0 & 1 & 0 & 0 & 0 & 0 & 0 & 0 & 0 & 0 & 0 & 0 & 0 & 0 & 0 & 0 & 0 & 0 & 0 & 0 & 0 & 0 & 0 & 0 \\
0 & 0 & 0 & 0 & 0 & 0 & 0.8 & 0.2 & 0 & 0 & 0 & 0 & 0 & 0 & 0 & 0 & 0 & 0 & 0 & 0 & 0 & 0 & 0 & 0 \\
0 & 0 & 0 & 0 & 0 & 0 & 0 & 0 & 0 & 0 & 0 & 0 & 0 & 0 & 0 & 0 & 0 & 0 & 0 & 0 & 0 & 0.5 & 0.5 & 0 & 0 \\
0 & 0 & 0.9 & 0 & 0.1 & 0 & 0 & 0 & 0 & 0 & 0 & 0 & 0 & 0 & 0 & 0 & 0 & 0 & 0 & 0 & 0 & 0 & 0 & 0 & 0 \\
0 & 0 & 0 & 0 & 0 & 0 & 0 & 0 & 0 & 0.9 & 0.1 & 0 & 0 & 0 & 0 & 0 & 0 & 0 & 0 & 0 & 0 & 0 & 0 & 0 & 0 \\
0 & 0 & 0 & 0 & 0 & 0 & 0 & 0 & 0 & 0 & 0 & 0 & 0 & 0 & 0 & 0 & 0 & 0.1 & 0.9 & 0 & 0 & 0 & 0 & 0 & 0 \\
0 & 0 & 0 & 0 & 0 & 1 & 0 & 0 & 0 & 0 & 0 & 0 & 0 & 0 & 0 & 0 & 0 & 0 & 0 & 0 & 0 & 0 & 0 & 0 & 0 \\
0 & 0 & 0 & 0 & 0 & 0 & 0 & 0 & 0 & 0 & 0 & 0 & 1 & 0 & 0 & 0 & 0 & 0 & 0 & 0 & 0 & 0 & 0 & 0 & 0 \\
0 & 0 & 0 & 0 & 0 & 0 & 0 & 0 & 0 & 0 & 0 & 0 & 0 & 0 & 0 & 0 & 0.5 & 0.5 & 0 & 0 & 0 & 0 & 0 & 0 & 0 \\
0 & 0 & 0 & 0 & 0 & 0 & 0 & 0 & 0.8 & 0 & 0.2 & 0 & 0 & 0 & 0 & 0 & 0 & 0 & 0 & 0 & 0 & 0 & 0 & 0 & 0 \\
0 & 0 & 0 & 0 & 0 & 0 & 0 & 0 & 0 & 0 & 0 & 0 & 0 & 0 & 1 & 0 & 0 & 0 & 0 & 0 & 0 & 0 & 0 & 0 & 0 \\
0 & 0 & 0 & 0 & 0 & 0 & 0 & 0 & 0 & 0 & 0 & 1 & 0 & 0 & 0 & 0 & 0 & 0 & 0 & 0 & 0 & 0 & 0 & 0 & 0 \\
0 & 0 & 0 & 0 & 0 & 0 & 0 & 0 & 0 & 0 & 0 & 0 & 0 & 0 & 0 & 0.1 & 0 & 0.9 & 0 & 0 & 0 & 0 & 0 & 0 & 0 \\
0 & 0 & 0 & 0 & 0 & 0 & 0 & 0 & 0.5 & 0.5 & 0 & 0 & 0 & 0 & 0 & 0 & 0 & 0 & 0 & 0 & 0 & 0 & 0 & 0 & 0 \\
0 & 0 & 0 & 0 & 0 & 0 & 0 & 0 & 0 & 0 & 0 & 0 & 0 & 1 & 0 & 0 & 0 & 0 & 0 & 0 & 0 & 0 & 0 & 0 & 0 \\
0 & 0 & 0 & 0 & 0 & 0 & 0 & 0 & 0 & 0 & 0 & 0 & 0 & 0 & 0 & 0 & 0 & 0.1 & 0 & 0.9 & 0 & 0 & 0 & 0 & 0 \\
0 & 0 & 0 & 0 & 0 & 0.4 & 0.4 & 0.2 & 0 & 0 & 0 & 0 & 0 & 0 & 0 & 0 & 0 & 0 & 0 & 0 & 0 & 0 & 0 & 0 & 0 \\
0 & 0 & 0 & 0 & 0 & 0 & 0 & 0 & 0 & 0 & 0 & 0 & 0 & 0 & 0 & 0.5 & 0.5 & 0 & 0 & 0 & 0 & 0 & 0 & 0 & 0 \\
0 & 0 & 0 & 0 & 0 & 0 & 0 & 0 & 0 & 0 & 0 & 0 & 0 & 0 & 0 & 0 & 0 & 0 & 0 & 0 & 0.1 & 0 & 0.9 & 0 & 0 \\
0 & 0 & 0.9 & 0.1 & 0 & 0 & 0 & 0 & 0 & 0 & 0 & 0 & 0 & 0 & 0 & 0 & 0 & 0 & 0 & 0 & 0 & 0 & 0 & 0 & 0 \\
0 & 0 & 0 & 0 & 0 & 0 & 0 & 0 & 0 & 0 & 0 & 0 & 0 & 0 & 0 & 0 & 0 & 0 & 0.1 & 0.9 & 0 & 0 & 0 & 0 & 0 \\
0 & 0 & 0 & 0 & 0 & 0 & 0 & 0 & 0 & 0 & 0 & 0 & 0 & 0 & 0 & 0 & 0 & 0 & 0 & 0 & 0 & 0 & 0 & 1 & 0 \\
1 & 0 & 0 & 0 & 0 & 0 & 0 & 0 & 0 & 0 & 0 & 0 & 0 & 0 & 0 & 0 & 0 & 0 & 0 & 0 & 0 & 0 & 0 & 0 & 0 \\
0 & 0 & 0 & 0 & 0 & 0 & 0 & 0 & 0 & 0 & 0 & 0 & 0 & 0 & 0 & 0 & 0 & 0 & 0 & 0 & 0.1 & 0.9 & 0 & 0 & 0
\end{bmatrix} \tag{A.2}$$

References

[1] Global EV outlook understanding the electric vehicle landscape to 2020. Available from: <https://www.iea.org/publications/globalevoutlook_2013.pdf> [accessed 07.21.16].

[2] US Department of Energy. Available from: <http://www.afdc.energy.gov/fuels/electricity_benefits.html> [accessed 09.20.16].

[3] Electric Vehicle Charging Information System. Available from: <http://www.ev.or.kr/eng> [accessed 09.13.16].

[4] Evaluating electric vehicle charging impacts and customer charging behaviors – Experiences from six smart grid investment grant projects. Available from: <https://www.smartgrid.gov/files/B3_revised_master-12-17-2014_report.pdf> [accessed 06.08.16].

[5] Salah F, Ilg J, Flath C, Basse H, van Dinther C. Impact of electric vehicles on distribution substations: a Swiss case study. Appl Energy 2015;137:88–96. http://dx.doi.org/10.1016/j.apenergy.2014.09.091.

[6] Wang H, Song Q, Zhang L, Wen F, Huang J. Load characteristics of electric vehicles in charging and discharging states and impacts on distribution systems. In: Sustainable power generation and supply (SUPERGEN) int conf, Hangzhou, China; 2012. p. 1–7, doi:http://dx.doi.org/10.1049/cp.2012.1837.

[7] Park WJ, Song KB, Park JW. Impact of electric vehicle penetration-based charging demand on load profile. J Electr Eng Technol 2013;8(2):244–51. http://dx.doi.org/10.5370/JEET.2013.8.2.244.

[8] Fernandez LP, San Roman TG, Cossent R, Domingo CM, Frias P. Assessment of the impact of plug-in electric vehicles on distribution networks. IEEE Trans Power Syst 2011;26(1):206–13. http://dx.doi.org/10.1109/TPWRS.2010.2049133.

[9] Valsera-Naranjo E, Sumper A, Villafafila-Robles R, Martinez-Vicente D. Probabilistic method to assess the impact of charging of electric vehicles on distribution grids. Energies 2012;5:1503–31. http://dx.doi.org/10.3390/en5051503.

[10] Olivella-Rosell P, Villafafila-Robles R, Sumper A, Bergas-Jane J. Probabilistic agent-based model of electric vehicle charging demand to analyse the impact on distribution networks. Energies 2015;8:4160–87. http://dx.doi.org/10.3390/en8054160.

[11] Valsera-Naranjo E, Martinez-Vicente D, Sumper A, Villafafila-Robles R, Sudria-Andreu A. Deterministic and probabilistic assessment of the impact of the electrical vehicles on the power grid. In: Proc IEEE power and energy soc general meeting. p. 1–8. http://dx.doi.org/10.1109/PES.2011.6039546.

[12] Shariff NBM, Essa MA, Cipcigan L. Probabilistic analysis of electric vehicles charging load impact on residential distributions networks. In: IEEE ENERGYCON. p. 1–6. http://dx.doi.org/10.1109/ENERGYCON.2016.7513943.

[13] Neaimeh M, Wardle R, Jenkins A, Yi J, Hill G, Lyons P, et al. A probabilistic approach to combining smart meter and electric vehicle charging data to investigate distribution network impacts. Appl Energy 2015;157:688–98. http://dx.doi.org/10.1016/j.apenergy.2015.01.144.

[14] Mu Y, Wu J, Jenkins N, Jia H, Wang C. A Spatial-Temporal model for grid impact analysis of plug-in electric vehicles. Appl Energy 2014;114:456–65. http://dx.doi.org/10.1016/j.apenergy.2013.10.006.

[15] Li Y, Davis C, Lukszo Z, Weijnen M. Electric vehicle charging in China's power system: energy, economic and environmental trade-offs and policy implications. Appl Energy 2016;173:535–54. http://dx.doi.org/10.1016/j.apenergy.2016.04.040.

[16] Temiz A, Guven AN. Assessment of impacts of electric vehicles on LV distribution networks in Turkey. In: IEEE ENERGYCON. p. 1–6. http://dx.doi.org/10.1109/ENERGYCON.2016.7514020.

[17] Xydas E, Marmaras C, Cipcipgan L, Jenkins N, Carroll S, Barker M. A data-driven approach for characterising the charging demand of electric vehicles: a UK case study. Appl Energy 2016;162:763–71. http://dx.doi.org/10.1016/j.apenergy.2015.10.151.

[18] Arias MB, Bae S. Electric vehicle charging demand forecasting model based on big data technologies. Appl Energy 2016;183:327–39. http://dx.doi.org/10.1016/j.apenergy.2016.08.080.

[19] Moon SK, Kim JO, et al. Balanced charging strategies for electric vehicles on power systems. Appl Energy 2017;189:44–54. http://dx.doi.org/10.1016/j.apenergy.2016.12.025.

[20] Capasso C, Veneri O. Experimental study of a DC charging station for full electric and plug in hybrid vehicles. Appl Energy 2015;152:131–42. http://dx.doi.org/10.1016/j.apenergy.2015.04.040.

[21] Deilami S, Masoum AS, Moses PS, Masoum MAS. Real-time coordination of plug-in electric vehicle charging in smart grids to minimize power losses and improve voltage profile. IEEE Trans Smart Grid 2011;2(3):456–67. http://dx.doi.org/10.1109/TSG.2011.2159816.

[22] Richardson DB. Electric vehicles and the electric grid: a review of modeling approaches, Impacts, and renewable energy integration. Renew Sustain Energy Rev 2013;19:247–54. http://dx.doi.org/10.1016/j.rser.2012.11.042.

[23] Veneri O, Capasso C, Iannuzzi D. Experimental evaluation of DC charging architecture for fully-electrified low-power two-wheeler. Appl Energy 2016;162:1428–38. http://dx.doi.org/10.1016/j.apenergy.2015.03.138.

[24] Bae S, Kwasinski A. Spatial and temporal model of electric vehicle charging demand. IEEE Trans Smart Grid 2012;3(1):394–403. http://dx.doi.org/10.1109/TSG.2011.2159278.

[25] Shrestha S, Hansen TM. Spatial-temporal stochasticity of electric vehicles in an integrated traffic and power system. In: IEEE EIT int conf. p. 227–32. http://dx.doi.org/10.1109/EIT.2016.7535245.

[26] Zhou Z, Lin T. Spatial and temporal for electric vehicle rapid charging demand. In: IEEE VPPC. p. 345–8. http://dx.doi.org/10.1109/VPPC.2012.6422675.

[27] Viswanathan V, Zehe D, Ivanchev J, Pelzer D, Knoll A, Aydt H. Simulation-assisted exploration of charging infrastructure requirements for electric vehicles in urban environments. J Comput Sci 2016;12:1–10. http://dx.doi.org/10.1016/j.jocs.2015.10.012.

[28] Bolch G, Greiner S, de Meer H, Trivedi KS. Queueing networks and markov chains. 2nd ed. New Jersey: John Wiley & Sons Inc; 2006.

[29] Iversen EB, Morales JM, Madsen H. Optimal charging of an electric vehicle using a Markov decision process. Appl Energy 2014;123:1–12. http://dx.doi.org/10.1016/j.apenergy.2014.02.003.

[30] Crisostomi E, Kirkland S, Shorten R. A google-like model of road network dynamics and its application to regulation and control. Int J Control 2011;84(3):633–51. http://dx.doi.org/10.1080/00207179.2011.568005.

[31] Mandelbrot B. How long is the coast of Britain? Statistical self-similarity and fractional dimension. Science 1967;156(3775):636–8.

[32] Cant RG. Changes in the location of manufacturing in New Zealand 1957–1968: An application of three-mode factor analysis. New Zealand Geogr 1971;27:38–55.

[33] Honarkhah M, Caers J. Stochastic simulation of patterns using distance-based pattern modeling. Math Geosci 2010;42(5):487–517. http://dx.doi.org/10.1007/s11004-010-9276-7.

[34] Tahmasebi P, Hezarkhani A, Sahimi M. Multiple-point geostatistical modeling based on the cross-correlation functions. Comput Geosci 2012;16(3):779–79742. http://dx.doi.org/10.1007/s10596-012-9287-1.

[35] Sang L, Zhang C, Yang J, Zhu D, Yun W. Simulation of land use spatial pattern of towns and villages based on CA-Markov model. Math Comput Model 2011;54(3–4):938–43. http://dx.doi.org/10.1016/j.mcm.2010.11.019.

[36] Banisch S, Lima R, Araújo T. Agent based models and opinion dynamics as Markov chains. Social Networks 2012;34(4):549–61. http://dx.doi.org/10.1016/j.socnet.2012.06.001.

[37] Jiang P, Liu X, Zhang J, Yuan X. A framework based on hidden Markov model with adaptive weighting for microcystin forecasting and early-warning. Decision Support Syst 2016;84:89–103. http://dx.doi.org/10.1016/j.dss.2016.02.003.

[38] Cerqueti R, Falbo P, Pelizzari C. Relevant states and memory in Markov chain bootstrapping and simulation. Eur J Operat Res 2017;256(1):163–77. http://dx.doi.org/10.1016/j.ejor.2016.06.006.

[39] Han G, Sohn K. Activity imputation for trip-chains elicited from smart-card data using a continuous hidden Markov model. Transp Res Part B: Methodol 2016;83:121–35. http://dx.doi.org/10.1016/j.trb.2015.11.015.

[40] Khadr M. Forecasting of meteorological drought using Hidden Markov Model (case study: The upper Blue Nile river basin, Ethiopia). Ain Shams Eng J 2016;7(1):47–56. http://dx.doi.org/10.1016/j.asej.2015.11.005.

[41] Epaillard E, Bouguila N. Proportional data modeling with hidden Markov models based on generalized Dirichlet and Beta-Liouville mixtures applied to anomaly detection in public areas. Pattern Recog 2016;55:125–36. http://dx.doi.org/10.1016/j.patcog.2016.02.004.

[42] Fernández C, Mateu C, Moral R, Sole-Mauri F. A predictor model for the composting process on an industrial scale based on Markov processes. Environ Model Software 2016;79:156–66. http://dx.doi.org/10.1016/j.envsoft.2016.02.007.

[43] Bojesen M, Skov-Petersen H, Gylling M. Forecasting the potential of Danish biogas production – spatial representation of Markov chains. Biomass Bioenergy 2015;81:462–72. http://dx.doi.org/10.1016/j.biombioe.2015.07.030.

[44] Saadi I, Mustafa A, Teller J, Cools M. Forecasting travel behavior using Markov Chains-based approaches. Transp Res Part C: Emerging Technol 2016;69:402–17. http://dx.doi.org/10.1016/j.trc.2016.06.020.

[45] Sagayaraj MR, Raj AM, Sathiyavani G. A study on Markov chain with transition diagram. Int J Tech Res Appl 2015;3(2):123–5.

[46] Bondy JA, Murty USR. Graph theory with applications. 1st ed. New York: Elsevier Science Publishing Co.; 1976.

[47] Porta S, Crucitti P, Latora V. The network analysis of urban streets: a dual approach. Physica A 2006;369(2):853–66. http://dx.doi.org/10.1016/j.physa.2005.12.063.

[48] Schlote A, Crisostomi E, Kirkland S, Shorten R. Traffic modelling framework for electric vehicles. Int J Control 2012;85(7):880–97. http://dx.doi.org/10.1080/00207179.2012.668716.

[49] Langville AN, Meyer CD. Google's PageRank and beyond. Princeton University Press; 2006.

[50] Rossi RA, Gleich DF. Dynamic PageRank using evolving teleportation. In: Proc int conf on algorithms and models for the web graph, Halifax, NS, Canada. p. 126–37. http://dx.doi.org/10.1007/978-3-642-30541-2_10.

[51] Seoul Transport Operation & Information Service (TOPIS). Available from: <http://topis.seoul.go.kr/#> [accessed 08.22.16].

[52] Ivanchev J, Aydt H, Knoll A. Spatial and temporal analysis of mismatch between planned road infrastructure and traffic demand in large cities. In: Intelligent transportation syst int conf, Washington, DC. p. 1463–70. http://dx.doi.org/10.1109/ITSC.2015.239.

[53] Cao Y, Tang S, Li C, Zhang P, Tan Y, Zhang Z, et al. An optimized EV charging model considering TOU price and SOC curve. IEEE Trans Smart Grid 2012;3(1):388–93. http://dx.doi.org/10.1109/TSG.2011.2159630.

[54] Tesla Supercharger. Available from: <https://www.tesla.com/supercharger> [accessed 01.10.17].

[55] Zhang P, Qian K, Zhou C, Stewart B, Hepburn D. A methodology for optimization of power systems due to electric vehicle charging load. IEEE Trans n Power Syst 2012;27(3):1628–36. http://dx.doi.org/10.1109/TPWRS.2012.2186595.

[56] Kulkarni VG. Introduction to modeling and analysis of stochastic systems. 2nd ed. New York: Springer; 2011.